Coral Photosymbiosis on Mid-Devonian Reefs

Working Paper

Author(s):
Jung, Jonathan; Zoppe, Simon; Söte, Till; Moretti, Simone; Duprey, Nicolas; Foreman, Alan; Wald, Tanja (iD); Vonhof, Hubert; Haug, Gerald; Sigman, Daniel; Schindler, Eberhard; Janussen, Dorte; Martínez-García, Alfredo

Coral Photosymbiosis on Mid-Devonian Reefs

Jonathan Jung (✉ jonathan.jung@mpic.de)

Max-Planck Institute for Chemistry   https://orcid.org/0000-0002-2739-9926

Simon Zoppe

Department of Geosciences, Goethe University

Till Söte

Department of Geology and Paleontology, University of Münster

Simone Moretti

Max Planck Institute for Chemistry   https://orcid.org/0000-0002-6772-7269

Nicolas Duprey

Max Planck Institute for Chemistry

Alan Foreman

Max-Planck Institute for Chemistry

Tanja Wald

Max-Planck Institute for Chemistry   https://orcid.org/0000-0002-1774-4749

Hubert Vonhof

Max Planck Institute for Chemistry   https://orcid.org/0000-0002-0897-8244

Gerald Haug

Max Planck Institute for Chemistry

Daniel Sigman

Princeton University   https://orcid.org/0000-0002-7923-1973

Eberhard Schindler

Senckenberg Research Institute and Natural History Museum Frankfurt

Dorte Janussen

Senckenberg Research Institute

Alfredo Martinez-Garcia

Max Planck Institute for Chemistry   https://orcid.org/0000-0002-7206-5079

Abstract

The ability of scleractinian corals to thrive in the oligotrophic (low-nutrient, low-productivity) surface waters of the tropical ocean is commonly attributed to their symbiotic relationship with photosynthetic dinoflagellates[1,2]. The evolutionary history of this symbiosis might clarify its organismal and environmental roles. It is currently unclear whether photosymbiosis first arose in the Triassic, with the emergence of scleractinian corals, or if it was already prevalent amongst older coral groups that have since gone extinct[3−5]. Here, we report the first measurements of nitrogen isotope ratios of coral-bound organic matter (CB-δ^{15}N) in samples from Mid-Devonian reefs (Givetian, ca. 385 Ma), which represent the oldest isotopic constraint on the evolution of photosymbiosis to date. The colonial tabulate and loosely colonial (dendroid) corals analyzed have low CB-δ^{15}N values (1.59‰±0.53‰ and 1.45±0.66‰, respectively) in comparison with co-occurring solitary rugose corals (4.38‰±1.34‰). The isotopic difference between Devonian colonial and solitary corals (2.86‰±0.86‰) is statistically indistinguishable from that observed between modern symbiont-bearing and symbiont-barren corals (3.38‰±1.05‰). From this evidence we infer that Mid-Devonian colonial tabulate and loosely colonial (dendroid) corals hosted active photosymbionts, while solitary rugose corals did not. The low CB-δ^{15}N values of the Devonian colonial tabulate and dendroid corals relative to the modern range suggest that Devonian reefs formed in biogeochemical regimes analogous to the modern oligotrophic subtropical gyres. Widespread oligotrophy during the Devonian likely may have promoted coral photosymbiosis, potentially explaining why Devonian reefs were the most productive reef ecosystems of the Phanerozoic.

Introduction

The Devonian (~419− 359 Ma) was a period of higher sea surface temperatures (23−32°C)[6−8] and atmospheric carbon dioxide (1000 − 2000 ppm)[9,10]. Unlike today, carbonate chemistry was dominated by calcite precipitation, likely due to the lower Mg/Ca ratios of seawater[11−13]. The Mid-Devonian hosted the most significant expansion of metazoan reefs in the Phanerozoic[9,14], and well-preserved reefs from this period are widespread across present-day Europe, North America, North Africa, Australia, Siberia and China. In the Devonian, these reefs bordered the Rheic Ocean, which lay at the southern margin of Laurussia and northern border of Gondwana (Fig. 1)[9,15−17]. Along the southern edge of Laurussia, these ancient reef communities reached their greatest extent and highest diversity during the Givetian stage (~387−382 Ma)[9,14]. These flourishing metazoan reefs were wiped out diachronically over the course of the Kellwasser Crisis during the late Frasnian (372.2 Ma)[18]. Afterwards, reefs were mainly built by cyanobacteria/algae but were present only in very reduced numbers until the end of the Famennian (D/C boundary)[19−21]. It has been hypothesized that the ability to host photosymbionts was paramount to the ecological success of ancient reef communities during the Givetian stage[3,9,22], and that the subsequent reef collapse during the Late Devonian was associated with a gradual loss of photosymbiotic associations[2,9,22,23]. However, there is still no clear consensus as to whether photosymbiosis was prevalent in the now-extinct coral groups of the Paleozoic[3,4,24].

Modern tropical scleractinian coral reefs are home to an intricate symbiotic network of highly diverse organisms[25,26]. Most prominently, an endosymbiotic relationship with single-celled photosynthetic dinoflagellates of the family Symbiodiniacea allows corals to recycle and retain nutrients and leverage them for organic carbon production, an approach that is particularly strategic in oligotrophic, nutrient-poor surface waters[1,2]. The endosymbiotic algae reside in the gastrodermis of the coral and utilize the host's metabolic N waste (NH_4^+) for photosynthesis[27−29]. Due to isotopic fractionation in de-amination and other metabolic reactions, this NH_4^+ is depleted in ^{15}N[27].In symbiont-barren coral species (as in heterotrophic organisms in general), the ^{15}N-depleted metabolic NH_4^+ is excreted, elevating the nitrogen isotopic composition (expressed as δ^{15}N = [(^{15}N/^{14}N)$_{sample}$ / (^{15}N/^{14}N)$_{air}$ - 1]*1000 in ‰) of the coral relative to the food source by 2−4‰[28−33]. In contrast, in symbiont-bearing corals, metabolic NH_4^+ is translocated from the coral host to the

endosymbionts and thus, retained within the coral host-symbiont system[32]. Consequently, the $\delta^{15}N$ of symbiont-bearing corals roughly reflects the $\delta^{15}N$ of the food source without significant isotopic offset[29,34,35]. This $\delta^{15}N$ difference between symbiont-bearing and symbiont-barren corals is reflected in the organic compounds bound within the walls of the coral's mineral skeleton[30,34−36]. Different lines of evidence suggest that the $\delta^{15}N$ of organic matter bound to the biomineral matrix of corals and other calcifying organisms can remain unaltered for millions of years[30,36−42]. Thus, coral-bound organic matter $\delta^{15}N$ (CB-$\delta^{15}N$) can be used to assess photosymbiotic activity in fossil corals[30,36].

Studies based on the analysis of CB-$\delta^{15}N$ have traced some form of photosymbiosis in fossilized scleractinian corals to the Upper Triassic (Norian Stage, ~212 Ma)[30,36]. Phylogenetic reconstructions based on correlated evolution placed the emergence of photosymbiosis in corals to the Permian (282.8 ± 16 Ma)[43]. However, research on ancient photosymbiosis in Paleozoic corals relies primarily on comparisons with modern Scleractinia, based on morphology[3,4,9,22] or carbon and oxygen isotopes[3,22,24,44], which have elicited different interpretations. Photosymbiosis correlates with several dimensions of morphology, such as growth form, corallite size, and level of corallite integration. For instance, most modern colonial corals harbor photosymbionts, whereas solitary corals rarely do[3,45]. As a result, some studies have concluded that Paleozoic solitary rugose corals were purely symbiont-barren, whereas colonial corals harbored photosymbionts[3,46]. However, some modern corals provide exceptions: Solitary corals of the genus *Fungia* are known to harbor zooxanthellae, while colonial corals of the genus *Tubastraea* are known to be fully heterotrophic[47]. Additionally, based on comparative growth rates, skeletal micromorphology, and their depth distributions, it has been suggested that none of the Paleozoic corals hosted photosymbionts[4,5]. Carbonate carbon and oxygen isotope measurements have been deemed inconclusive, due to the potential for diagenetic alteration[30,48,49] and insufficient experimental data on the comparability of carbon and oxygen isotopes between calcitic (e.g., Paleozoic coral) and aragonitic (e.g., modern Scleractinian) corals[50,51].

Here, we present the first analysis of ancient photosymbiosis in Paleozoic corals using CB-$\delta^{15}N$ in samples from Mid-Devonian reefs. The studied coral samples are from the lower to middle Givetian, from the Hagen Balve Reef at Binolen (north-western Sauerland) and from the Eifel region (Sötenich and Dollendorf Synclines) in Germany (Fig. 1). We focused mainly on tabulate corals, loosely colonial (dendroid) and solitary rugose corals, as well as the carbonate sediment matrix in which they were buried (Figs. 2, 3 and Extended Data Fig. 1). The Paleozoic CB-$\delta^{15}N$ data are interpreted in the context of CB-$\delta^{15}N$ data from modern pairs of symbiont-bearing (i.e., *Porites* spp.) and symbiont-barren (i.e., *Tubastraea* spp.) coral species living in the same reef environment and depth, across a range of reef locations characterized by different 'baseline' $\delta^{15}N$ conditions (Fig. 4, Extended Data Fig. 2). In addition to CB-$\delta^{15}N$, coral skeleton $\delta^{18}O$ and $\delta^{13}C$ were measured in all Mid-Devonian and modern samples (Extended Data Fig 3).

The analysis of the N isotopic composition of organic matter bound to the biomineral matrix of fossil corals requires chemical cleaning to remove organic matter on the surface of the carbonate material, which may have undergone N isotopic alteration by diagenesis and/or may include exogenous N from natural processes or from contamination by sampling. A comparison between cleaned and uncleaned samples from Binolen shows large differences in the mean CB-$\delta^{15}N$ and weight-normalized N content, as well as in the variance of these measurements (Fig. 3). In general, uncleaned samples show higher and more variable CB-$\delta^{15}N$ and weight-normalized N content than do cleaned samples (see Methods). For example, the dendroid rugose coral samples have an average weight-normalized N content that is seven times higher in uncleaned samples than in cleaned samples, and tabulate and solitary rugose corals show on average two times higher weight-normalized N content in uncleaned samples, suggesting significant contamination from allochthonous organic matter.

These findings raise concerns about N isotopic reconstructions from the Paleozoic or earlier that rely on measurements of total sedimentary N or of components of sedimentary N that would have been exposed to exogenous N sources during deposition or through geologic time. Previous attempts to reconstruct changes in the Devonian N cycle have been based on

measurements of bulk sediment $\delta^{15}N$[52,53]. These studies suggested a larger range in, and a more negative average value for, $\delta^{15}N$ (-3‰ to 3‰)[52,53] than the cleaned coral-bound measurements reported here. Even in more recent sediments, bulk sediment $\delta^{15}N$ can be severely altered by diagenesis or contaminated by exogenous nitrogen[54–59]. Our unclean samples show negative and variable $\delta^{15}N$ values that fall in the range of those obtained for bulk sediment in previous studies[52,53]. However, these converge to a narrow, positive $\delta^{15}N$ range in the cleaned coral samples (Fig. 3). We limit our paleoecological and paleoenvironmental interpretation to measurements of cleaned samples, which reflect the fraction of organic matter that is protected from diagenesis by the biomineral matrix.

In the samples from the Hagen Balve reef at Binolen, we obtain a mean $\delta^{15}N$ of 1.85±0.56‰ for cleaned tabulate corals (*Roemerolites brevis rhiphaeus*) and 1.45±0.66‰ for cleaned dendroid rugose corals (*Dendrostella trigemme*) (Fig. 4a). In contrast, solitary rugose coral samples show a significantly higher $\delta^{15}N$ (P < 0.01), with mean values of 5.16±0.88‰ for *Temnophyllum latum,* 5.52±1.49‰ for *Temnophyllum astrictum*, and 3.57±0.22‰ for an unidentified rugose coral sample. The samples from the Sötenich Syncline in the Eifel show a very similar pattern, with mean $\delta^{15}N$ values of 1.22±0.08‰ for the tabulate coral *Roemerolites brevis brevis* and significantly higher $\delta^{15}N$ values (P < 0.01) for the solitary rugose coral *Temnophyllum latum* (4.01±0.42‰) (Fig. 4a).

The CB-$\delta^{15}N$ values obtained for different individuals of the colonial species *Romerolites brevis rhiphaeus* (1.85±0.56‰) and *Dendrostella trigemme* (1.45±0.66‰) at the Hagen Balve reef were statistically indistinguishable from those obtained in a single individual of *Romerolites brevis brevis* from the Sötenich Syncline (1.22±0.08‰). Similarly, the average CB-$\delta^{15}N$ value of multiple species of solitary rugose corals measured at the Hagen Balve reef (4.62±1.24‰) was close to those measured from the Sötenich (4.01±0.42‰) and Dollendorf (3.06±0.47‰) Synclines in the Eifel region. This is a significant finding, given that the two sites experienced very different diagenetic histories. The Conodont Alteration Index (CAI) indicates that samples from the Hagen Balve Reef experienced maximum temperatures of 190–300°C (Supplementary Table 1) while the temperatures experienced by samples from the Eifel region did not exceed 50–95°C[60]. The similarity of the CB-$\delta^{15}N$ in these two locations is consistent with results from laboratory heating experiments, which show no significant changes in CB-$\delta^{15}N$ despite significant decreases in weight-normalized N content at temperatures of 300°C[40], suggesting that loss of partially exposed N does not significantly alter the N isotopic composition of the remaining organic matter. CB-$\delta^{15}N$ values of our Binolen and Eifel samples show no correlation with N content, further supporting this interpretation (Extended Data Fig. 7). The consistency in the $\delta^{15}N$ values obtained for the different species of colonial and solitary corals at different sites, as well as the lack of correlation between weight-normalized N content and CB-$\delta^{15}N$, strongly suggest that the measured coral-bound organic matter is indeed native to the organisms and is isotopically unaltered during its long residence in the geological record and the wide range of temperatures experienced by these fossils.

The average CB-$\delta^{15}N$ difference of solitary rugose corals from colonial tabulate and rugose corals ($\Delta\delta^{15}N_{S-C}$) was statistically significant (P < 0.01) and remarkably similar between samples from the Hagen Balve Reef ($\Delta\delta^{15}N_{S-C}$ = 3.10±1.09‰), and the Eifel region ($\Delta\delta^{15}N_{S-C}$ = 2.51±0.40‰). These isotopic differences are also similar to those observed between modern symbiont-barren and symbiont-bearing corals ($\Delta\delta^{15}N_{BA-BE}$) living in the same reef environments (average $\Delta\delta^{15}N_{BA-BE}$ = 3.38±1.05‰) (Fig. 4d, Extended Data Fig. 4). Our modern dataset demonstrates that the isotopic difference between symbiont-barren and symbiont-bearing corals is consistent across reef systems characterized by different baseline $\delta^{15}N$ values for their nitrate supply (Fig. 4c, Extended Data Fig. 2). The lowest average $\Delta\delta^{15}N_{BA-BE}$ values were found in corals from Socotra ($\Delta\delta^{15}N_{BA-BE}$ = 1.97‰) and Cape Verde ($\Delta\delta^{15}N_{BA-BE}$ = 2.35‰), and the highest average $\Delta\delta^{15}N_{BA-BE}$ was observed in Hong Kong ($\Delta\delta^{15}N_{BA-BE}$ = 5.02‰), while corals from Jamaica ($\Delta\delta^{15}N_{BA-BE}$ = 4.26‰), Colombia ($\Delta\delta^{15}N_{BA-BE}$ = 3.14‰) and Brazil ($\Delta\delta^{15}N_{BA-BE}$ = 3.51‰), showed values closer to the mean $\Delta\delta^{15}N_{BA-BE}$ (Extended Data Fig. 5). The observed differences in the magnitude of the species offsets may relate to the efficiency of

nutrient recycling by coral symbionts, the feeding behavior of the corals, or the degree of nitrate assimilation by coral symbionts[33,34,36,61,62]. In any case, the $\Delta\delta^{15}N_{BA-BE}$ valuesare consistent in all cases with expectations from the retention of a significant part of metabolic NH_4^+ within the host-symbiont system of symbiont-bearing corals, further supporting $\Delta\delta^{15}N_{BA-BE}$ as a distinctive marker for the presence/absence of coral photosymbionts[29,30,36,63].

The average $\Delta\delta^{15}N_{S-C}$ observed in Mid-Devonian samples from the Hagen Balve reef and the Eifel regions (average $\Delta\delta^{15}N_{S-C}$ = 2.86±0.86‰) is statistically indistinguishable (*P* = 0.459, Welch's t-test) from the $\Delta\delta^{15}N_{BA-BE}$ observed in modern corals (average $\Delta\delta^{15}N_{BA-BE}$ = 3.38‰±1.05‰) (Fig. 4b and 4d, Extended Data Fig. 4). Thus, our CB-$\delta^{15}N$ measurements indicate that tabulate and loosely colonial rugose corals hosted active photosymbionts, whereas solitary rugose corals did not. This is thus the oldest geochemical expression of the presence of photosymbiotic associations in corals to date, expanding the record by ~170 Ma, and suggests that autotrophic and heterotrophic corals co-existed on extinct reefs much as they do today.

Interestingly, the $\delta^{15}N$ values of the cleaned sedimentary matrix from Binolen (1.57±0.46‰), the Sötenich Syncline (1.27±0.16‰) and the Dollendorf Syncline (0.83±0.13‰) were similar to those of colonial or dendroid rugose coral samples (Fig. 4a). The sedimentary matrix consists mainly of fine bioclastic debris with abundant micrite. This bioclastic debris is likely dominantly sourced from the major calcifiers, including tabulate corals and loosely-colonial (dendroid) rugose corals, on the Hagen Balve Reef at Binolen[64], consistent with their photosymbiosis increasing their growth rate. Thus, the similarity of the sedimentary matrix $\delta^{15}N$ to that of the colonial corals may simply reflect that the matrix is largely composed of the remains of these corals. Our findings raise the possibility that, unlike bulk sediment measurements, the analysis of the mineral-bound N isotopic composition of sedimentary rocks rich in biogenic carbonate might provide robust information about past changes in the N cycle even when they do not contain recognizable macrofossils, provided that the surficial organic N on the biomineral grains is removed by chemical cleaning. If confirmed, this type of measurement may provide a new lens to investigate changes in the N cycle across broad ranges of geologic time and paleoenvironments.

The low average value for $\delta^{15}N$ reported here may offer insight into ocean N cycling during the Mid-Devonian. The $\delta^{15}N$ of corals is sensitive to the $\delta^{15}N$ of the fixed N supplied to their oligotrophic reef environment, which is typically dominated by the nitrate supplied from the shallow subsurface by mixing and/or upwelling[34,65], with exceptions in coastal systems with large terrestrial (including anthropogenic) N sources[61,66–68]. Accordingly, the large range in CB-$\delta^{15}N$ values among our modern sampling sites can be attributed to distinct processes in the marine N cycle that affect the $\delta^{15}N$ of N supplied to each reef (Extended Data Fig. 2). CB-$\delta^{15}N$ values are lowest from Jamaica (CB-$\delta^{15}N$ = 2.87±0.28‰), which is located in the central Caribbean. In this region, the $\delta^{15}N$ of the nitrate supply to the euphotic zone is low, largely due to regional N_2 fixation and its remineralization to low-$\delta^{15}N$ nitrate in the thermocline[69,70]. In contrast, the highest values were obtained from two nutrient-rich systems: Socotra (CB-$\delta^{15}N$ = 10.59±0.38‰) and Hong Kong (CB-$\delta^{15}N$ = 10.66±0.90‰) (Fig. 4c). Socotra is located in the vicinity of one of the largest oceanic oxygen-deficient zones, with high water-column denitrification rates, a process that strongly discriminates against ^{15}N and elevates the $\delta^{15}N$ of the subsurface nitrate that is supplied to the surface[71]. The estuary outside of Hong Kong, on the other hand, is influenced by anthropogenic activities in the Pearl River basin that tend to elevate the $\delta^{15}N$ of both ammonium and nitrate sources (e.g., ammonium oxidation coupled to denitrification)[61,63]. CB-$\delta^{15}N$ values from Colombia (CB-$\delta^{15}N$ = 5.96±1.51‰) and Cabo Verde (CB-$\delta^{15}N$ = 6.83±0.20‰) show intermediate values that are characteristic of mean ocean pycnocline nitrate[72,73].

Devonian mean CB-$\delta^{15}N$ values of colonial corals from the initial Hagen Balve Reef at Binolen (1.53±0.58‰) and the Sötenich Syncline (1.22±0.08‰) of the Eifel region are similar to, but lower, than those found in the western tropical and subtropical North Atlantic[35,74], a region dominated by strong density stratification, surface nutrient depletion, and low surface chlorophyll concentrations. The low $\delta^{15}N$ of the thermocline nitrate in this region, and similar nitrate isotopic

features in other subtropical gyres[75,76], likely derives from N_2 fixation, which is largely restricted to nitrogen-deplete surface waters[77] and which lowers thermocline nitrate $\delta^{15}N$ most strongly in the low-nutrient subtropical gyres[70]. Thus, the low CB-$\delta^{15}N$ that we observe in each of the fossil reefs may suggests that they occurred in a nutrient-poor environment associated with a westward-intensified subtropical gyre. This supports the view that the reefs of the Givetian (~385 Ma), which comprised one of the most widespread reef biota and diversity in the Phanerozoic, were adapted to nutrient-poor conditions, as applies broadly to the symbiont-bearing scleractinian coral reefs of today[9,19−21]. Thus, the success of symbiotic corals in the Givetian may have been linked to the occurrence of extensive coastal regions under the influence of strongly stratified, nutrient-poor conditions that characterize western ocean margins at tropical and subtropical latitudes.

However, the Givetian corals have CB-$\delta^{15}N$ values that are even lower than those measured in any modern coral specimen. The very low mean CB-$\delta^{15}N$ measured in the Givetian has several possible explanations. First, it may reflect natural environmental isotopic gradients. For example, the Givetian may have been characterized by intensification of the low-$\delta^{15}N$ features associated with tropical and subtropical waters. This might have occurred if N_2 fixation rates were greater and/or if the subtropical gyres were more expansive and characterized by a deeper thermocline. Subtropical gyre expansion may have been driven by the warm climate of the Givetian, consistent with climate model experiments of warming in which the atmospheric Hadley Cells expand[78,79]. If so, our data point to an aspect of global warming that may prove favorable for coral reef survival under highly oligotrophic conditions. A particularly deep western thermocline may also have been encouraged by the very wide ocean basin of the Givetian (Fig. 1). Alternatively, the low CB-$\delta^{15}N$ of the Givetian may reflect a global mean ocean nitrate $\delta^{15}N$ that was lower than modern. One possible mechanism would be a reduction in importance of water column denitrification in oceanic N loss[80], such as would be associated with reduced ocean suboxia. This would be consistent with observations of minimal water-column denitrification during warm periods of the Cenozoic, which imply that ocean suboxia is reduced under warmer climates[37,42].

Materials and Methods

Geological Setting and Stratigraphy

The main material was collected near a cliff at the top of the Binolen section ("C-Layers" after Löw et al., 2022; GPS: 51°22′12″N, 7°51′27″E) within the Hönne Valley in north-western Sauerland, Germany. The Binolen section is located in the northern Rhenish Massif at the eastern edge of the Remscheid-Altena Anticline, which is surrounded by carbonate platform deposits of the Hagen Balve Reef. In terms of stratigraphy, the base of the Binolen section was positioned into the lower Givetian (likely within the *timorensis* conodont zone), defining the lower boundary of the basal part of the Hagen-Balve Formation (Binolen Member)[64]. However, the cliff at the top of the Binolen Member falls within the lower/middle Givetian boundary interval[64,81].

During the Givetian, the Hagen Balve Reef was developed as an elongated carbonate platform surrounding a local submarine high on the Rhenish shelf, at the southern tip of Laurussia (Fig. 1). The onset of reef formation started approximately isochronous during the lower Givetian[1]. The depositional history of the initial reef formation of the Binolen Member was divided into several depophases[1]. The samples analyzed in this study were collected from strata within the upper part of Depophase VI (Beds 59 to 65 of "C-layers")[64] and stem from the initial reef platform of the Hagen Balve Reef. This part of the initial reef formation of the Binolen Member is characterized by coral-stromatoporoid frame-rudstones and coral-stromatoporoid-dominated float-bafflestones, representing a semi-open carbonate platform with argillaceous sediment input[64].

Samples from the Eifel were provided by the Senckenberg Research Institute and Natural History Museum Frankfurt. The limestone synclines of the Eifel are located between the Lower Rhine Bay in the north and the Trier Bay in the south.

Geologically, the region is part of the Rhenish Massif and consists of Devonian slates, sandstones, and limestones, interspersed with bioclasts, which were deposited in a coastal setting south of Laurussia (Fig. 1)[82,83].

The Sötenich Syncline is characterized by changing assemblages of thin layered marly mudstones and thick layers of gastropod-coral-trilobite wackestones to floatstones which merge into stromatoporoid -coral-rudstones in the uppermost profiles. The coral associations are indicative of a low energy regime within a shallow marine lagoon. Faunal composition and facies types in the upper profiles suggest elevated sediment input and elevated nutrient supply[83].

The Dollendorf Syncline yields a rich macrofauna characteristic of the Mid-Devonian. Local limestones are mainly composed of calcisphere-ostracod-wackestones or packestones and amphiporoid-floatstones, indicating a shallow marine lagoonal setting with restricted, low-energy water flow. Interspersed amphiporoid-rudstones suggest periods of high-energy regimes with potentially greater influence of open-marine conditions[82].

Thin Section Analyses and Sample Storage

For taxonomic identification of collected coral samples from Binolen, fossil-rich rock samples were cut systematically for longitudinal- and cross-sections of individual coral skeletons. Thin sections were prepared with a thickness of 50 mm. Microphotographs were made under transmitted light with a Keyence VHX digital microscope to identify the analyzed tabulate and rugose corals[84–86].

Nine thin sections from the initial Hagen Balve Reef at Binolen will be stored in the Geomuseum of the Westfälische Wilhelms University in Münster (GMM) under the inventory numbers GMM B2C.59-1 to GMM B2C.59-9.

Eifel samples were provided by the Senckenberg Research Institute and Natural History Museum Frankfurt, Germany, with *Roemerolites brevis brevis* from the Sötenich Syncline: SMF 40159; T*emnophyllum* cf. *ornatum* (= *T. latum*) from the Sötenich Syncline: SMF 40367/2 and *Mesophyllum vesiculosum* from the Dollendorf Syncline: SMF 73856.

Conodont Alteration Index (CAI)

The assessment of the textural alteration of conodonts as a proxy for the maturation of rocks has long been known[87]. The first systematic approach on quantifying temperature regimes a rock has experienced during diagenesis with the CAI dates back to 1977[88,89]. Generally, conodont elements are composed of calcium phosphate (frankolite)[87]. During the growing phase of the conodont animal, frankolite lamellae are separated by thin organic layers. This organic matter can alter as a consequence of a carbonization reaction and change color in a characteristic way known as the CAI (Extended Data Fig. 6, Supplementary Table 1). Since then, many authors successfully applied the CAI to assess and quantify the maturation of regional rock formations and basins[90–96].

The CAI has been used within the Rhenish Massif[93,97]. Helsen and Königshof (1994) yielded a useful map of CAI isoclines for the region. We used 30 conodonts from Binolen to determine the temperature-induced diagenetic overprint of the limestones which have been collected from slightly older strata only a few meters away and narrowed values down to 4.0–4.5 (which correspond to maximum temperatures of 190–300°C)[98] for most of the Middle Devonian strata of the Rhenish Massif. The CAIs of the different synclines of the Eifel Hills yield nearly homogenous values between 1.5–2.0 (which correspond to maximum temperatures of 50–95°C)[60,93,99].

Analysis of Coral-Bound Nitrogen Isotopes

The CB-δ^{15}N measurements were performed in the Martínez-García Lab at the Max-Planck Institute for Chemistry in Mainz (MPIC). We used the persulfate oxidation-denitrifier method[74,100], first applied to corals by Wang et al. (2014, 2015)[33,101], with the analytical modifications described by Moretti et al.[102].

The collected samples of fossil-rich carbonate rocks were cut into smaller handpieces using a stationary rock saw. Sample material was carefully extracted from the handpieces with a mm-drill bit attached to a hand-Dremel®. Only those specimens were considered that were located on the edge of a handpiece to ensure that the different phases of material (coral skeleton, secondary sparite and surrounding carbonate sediment) and their respective dimensions were visible (Fig. 2 and Extended Data Fig. 1). Each phase was collected exclusively from the center of mass to minimize contamination of adjacent material (Extended Data Fig. 1). Subsequent samples were sieved to separate coarse (250–63 µm) and fine (63–5 µm) aliquots. The coarse fraction was used for N-isotope analysis, while the fine fraction was further prepared for C- and O-isotope analysis.

Twenty mg (±2 mg) of unclean, coarse powder was weighed into a 12 ml Wheaton® tube. Subsequently, for the removal of clay particles, 10 ml of a 2% Na-Polyphosphate solution was added, left on a shaker at 120 rpm for five minutes and then put in an ultrasonic bath for one minute. Afterwards, the tubes were taken out and the supernatant was decanted. 8–10 ml of Milli-Q® water was added and samples were centrifuged at 300 rpm for two minutes before being removed. The procedure was repeated three times.

To remove potential Fe-Mn oxides, 5 ml of pH-adjusted dithionite-citric acid (pH 8) was added to each sample tube, which was placed in an 80°C DI-water bath for 30-40 min. The samples were removed and centrifuged, the supernatant was decanted, and the sample was rinsed three times with Milli-Q® (see steps above). Afterwards, sample material was transferred to a previously muffled 4 ml VWR® borosilicate glass vial and 3 ml of a potassium peroxydisulfate oxidative reactant (POR) solution (pH>12) was added. Samples were then autoclaved at 121°C for 65 min for the oxidation of non-bound organic matter. Finally, the supernatant was removed with a muffled pipette attached to a vacuum line set at 500 mbar, and the sample was rinsed at least three times with Milli-Q® until the supernatant reached pH 7. Cleaned samples were stored in a drying oven at 60°C overnight.

Once the powder had dried fully, 15±5 mg of cleaned powder was weighed inside an in-house clean room to minimize the opportunity for contamination. Thereafter, skeletal organic matter was released by dissolving the cleaned coarse powder with 4N hydrochloric acid (HCl). This leads to a solution of calcium chloride ($CaCl_2$) at pH < 2. The amount of 4N acid used had been calculated based on the sample weight. We used the stoichiometric calculation of the reaction ($CaCO_3 + 2HCl \rightleftharpoons CaCl_2 + H_2O + CO_2$), which translates to 5µl 4N HCl per 1 mg of clean carbonate powder. We added an additional 20 µl 4N HCl to each sample to ensure very low pH and thus complete dissolution.

Concurrently, a new POR solution was prepared inside the cleanroom with a 4 ml spike of 6.25N NaOH to reach high pH. 1 ml of POR solution was pipetted to each dissolved sample and at least 10 empty cleaned vials (blanks), and the batch of vials was placed in a custom-built sample rack that was tightly sealed with a PTFE sheet before being autoclaved at 121°C for 65 min. The basic POR pH conditions convert the sample N to nitrate within the closed vial. After the autoclave run, supernatant was tested for pH to make sure every sample is basic (pH > 10). Eventually, each sample was balanced with the same HCl aliquot previously used for dissolution to reach a pH near 7. From the resulting aliquot, nitrate concentration was measured for each sample by quantitative conversion to nitric oxide and subsequent chemiluminescence detection[103], and these measurements were used to calculate the sample volume yielding 5 nmol N of nitrate.

A volume of 1 ml of concentrated denitrifying bacteria (*Pseudomonas chlororaphis*) was injected into 800 ml of growth media and left 4–6 days to grow in the dark at room temperature on a shaking rack. Once the bacteria have grown sufficiently, the medium was transferred to autoclaved PE bottles and centrifuged at 7600 rpm for 10 minutes. The supernatant was then discarded and the remaining bacteria pellet was resuspended with a buffered (pH 6.3) resuspension medium. From this, 3 ml was pipetted into muffled 12 ml glass vials, capped with a septum and tightly sealed were placed upside-down on a needle rack with a small extra needle for pressure release. The needle rack supplied a continuous flow of N_2 for at least three hours to replace the internal atmosphere and dissolved gases with pure N_2. Bacteria vials were removed from the rack, and ~0.8 ml of the oxidized sample was injected into each bacteria vial. Once all samples have

been injected, bacteria vials were placed in the dark for 2–3 hours to ensure quantitative transformation of nitrate to nitrous oxide before being frozen at -21°C.

On the day of analysis, bacteria were thawed, lysed with several drops of 10N NaOH and finally placed on a mass spectrometer for isotope analysis. The $\delta^{15}N$ of the N_2O was determined by a purpose-built inlet system coupled to a Thermo MAT253 Plus stable isotope ratio mass spectrometer[100,104]. Long-term precision was determined by running internal carbonate standards with each sample batch, which yielded an average carbonate standard reproducibility of ±0.2‰. Average reproducibility for replicate Devonian coral measurements was 0.22‰ (n=45) and 0.68‰ (n=20) for clean and unclean samples, respectively.

Modern samples of *Tubastraea* spp. and *Porites* spp. were taken from four different collections in the Senckenberg Research Institute and Natural History Museum Frankfurt. Subsequent samples were drilled with a hand-held Dremel® and powder was transferred into 4ml borosilicate glasses using aluminum foil. Each sample was then sieved into coarse (250–63 μm) and fine (63–5 μm) aliquots, where 6 mg coarse and 100–200 μg fine powder was used for N isotope and C/O isotope analysis, respectively.

Before analysis of modern coral samples, 8 mg of clean coarse powder was weighed into a 4 ml VWR® borosilicate glass vial and filled with 4.25 ml of 2% Na-hypochlorite before being left on a shaking table at 120 rpm for at least 24 hours. Afterwards, supernatant was removed with a muffled pipette attached to a vacuum line set at 500 mbar and was further treated the same as described with the Paleozoic samples.

Coral Oxygen and Carbon Isotopes

Amounts of 100–200 μg of coral carbonate sample material was analyzed for $\delta^{18}O$ in the inorganic stable isotope laboratory at the Max-Planck-Institute for Chemistry in Mainz. Within a run of 55 samples, one international carbonate standard (IAEA-603, n=10) and one internal carbonate standard (VICS, n=11) were used to calibrate the analyses to the Vienna Pee Dee Belemnite (VPDB) scale. Samples were measured with an isotope ratio mass spectrometer (IRMS) (Delta V Advantage, Thermo Scientific, Bremen, Germany) which is connected to a GasBench II unit (Thermo Scientific). Each sample was placed in a 12ml exetainer vial (Part no. 9RK8W; Labco, Lampeter, UK). Samples and standards were then put into a 70°C-heated hot block. Firstly, vials were flushed with He to remove atmospheric CO_2. Then, 5-10 drops of >99% H_3PO_4 were added and the sample was left to dissolve for 1.5 hours. Finally, the sample was transferred in He carrier gas to the GasBench II, where water and contaminant gases were removed before subsequent isotope analysis in the IRMS. Average analytical precision, based on the reproducibility of IAEA-603, was 0.11‰ (1SD, n=42) and 0.09‰ (1SD, n=42) for oxygen and carbon isotopes, respectively.

The $\delta^{18}O$ and $\delta^{13}C$ values for our Paleozoic samples show mean $\delta^{18}O$ values ranging from -5.57‰ for secondary sparite to -6.64‰ for sediment samples (Supplementary Table 4). Mean $\delta^{13}C$ values of all samples cluster around 1.95‰, where lowest $\delta^{13}C$ values are recorded for dendroid rugose corals (1.17‰), whereas sediment and secondary sparite show higher $\delta^{13}C$ values (2.39‰ and 2.29‰, respectively). Notably, solitary rugose coral samples cluster within narrow $\delta^{18}O$ and $\delta^{13}C$ values (-5.72‰ and 1.52‰, respectively).

Skeletal $\delta^{18}O$ and $\delta^{13}C$ values of modern samples are relatively widespread ranging from -7.39‰ to 3.57‰ and -10.27‰ to 1.60‰, respectively (Supplementary Table 5). Symbiont-bearing and symbiont-barren coral species do not show a distinct offset in either $\delta^{18}O$ or $\delta^{13}C$. However, modern symbiont-bearing and -barren species can be distinguished in a cross-plot of $\delta^{18}O$ vs $\delta^{13}C$[44] (Extended Data Fig. 3).

The original oxygen and carbon isotopic composition of corals can be altered by partial dissolution of aragonite, precipitation of secondary carbonates or by recrystallisation of metastable aragonite to calcite (McGregor and Gagan,

2003; Müller et al., 2001; Sayani et al., 2011; Swart, 2015). While secondary carbonates (sparite) are predominantly observed in submarine environments[107], partial dissolution or recrystallisation is more common for subaerial settings (Hendy et al., 2007; McGregor and Gagan, 2003). According to previous studies on the Hagen Balve Reef and the Eifel region, samples have probably experienced both, submarine and subaerial alteration[64,82,83].

$\delta^{18}O$ and $\delta^{13}C$ values of our samples from Binolen and the Eifel cluster within the range previously discussed for marine limestones[111]. The narrow range of $\delta^{18}O$ and $\delta^{13}C$ values would suggest photosymbiosis across species[24,44,112] and thus, would stand in direct contrast to our result from CB-$\delta^{15}N$ measurements, and previous suggestions, based on morphological analysis, that no Paleozoic corals harbored symbionts[4,5] (Extended Data Fig. 3). Previous studies have highlighted that diagenetic processes and geochemical comparisons of polymorphs (i.e., calcitic skeleton for Paleozoic coral samples and aragonitic skeleton for modern Scleractinia) can bias the interpretation of $\delta^{18}O$ and $\delta^{13}C$ values and thus, are thought to be less robust proxies for fossil reef settings[49,106,109]. In addition, increasing temperatures and recrystallization can bias carbonate oxygen isotope values towards more negative $\delta^{18}O$ values[113,114]. Thus, it is possible that diagenetic alteration of the coral carbonate $\delta^{18}O$ can bias the interpretation towards more symbiotic associations.

Statistical Analysis

Standard deviations are given as ±1SD and statistical significance tests were conducted either by a Welch's t-test given a similar sample size and a heterogenous variance or an individual t-test for similar sample sizes and variances[115,116]. All analyses were conducted using Python3 on a Jupyter Notebook® (version 5.7.4). Data were imported using the Pandas library and plotted with Seaborn or Matplotlib libraries.

Declarations

Code availability

Codes used for figures and data analyses are available on GitHub (https://github.com/marinejon/Coral-Photosymbiosis-on-Mid-Devonian-Reefs.git).

References

1. Davy, S. K., Allemand, D. & Weis, V. M. Cell Biology of Cnidarian-Dinoflagellate Symbiosis. *Microbiol. Mol. Biol. Rev.* **76**, 229–261 (2012).

2. Fournier, A. The story of symbiosis with zooxanthellae, or how they enable their host to thrive in a nutrient poor environment. 8 (2013).

3. Coates, A. G. & Jackson, J. B. C. Clonal Growth, Algal Symbiosis, and Reef Formation by Corals. *Paleobiology* **13**, 363–378 (1987).

4. Scrutton, C. T. The Palaeozoic corals, II: structure, variation and palaeoecology. *Proceedings of the Yorkshire Geological Society* **52**, 1–57 (1998).

5. Scrutton, C. T. The Palaeozoic corals, I: origins and relationships. *Proceedings of the Yorkshire Geological Society* **51**, 177–208 (1997).

6. Copper, P. & Scotese, C. R. Megareefs in Middle Devonian supergreenhouse climates. in *Extreme depositional environments: mega end members in geologic time* (eds. Chan, M. A. & Archer, A. W.) vol. 370 0 (Geological Society of America, 2003).

7. Joachimski, M. M. *et al.* Devonian climate and reef evolution: Insights from oxygen isotopes in apatite. *Earth and Planetary Science Letters* **284**, 599–609 (2009).

8. Ries, J. B. Review: geological and experimental evidence for secular variation in seawater Mg/Ca (calcite-aragonite seas) and its effects on marine biological calcification. *Biogeosciences* **7**, 2795–2849 (2010).

9. Bridge, T. C. L., Baird, A. H., Pandolfi, J. M., McWilliam, M. J. & Zapalski, M. K. Functional consequences of Palaeozoic reef collapse. *Sci Rep* **12**, 1386 (2022).

10. Mora, C. I., Driese, S. G. & Seager, P. G. Carbon dioxide in the Paleozoic atmosphere: Evidence from carbon-isotope compositions of pedogenic carbonate. *Geology* **19**, 1017–1020 (1991).

11. Lowenstein, T. K., Timofeeff, M. N., Brennan, S. T., Hardie, L. A. & Demicco, R. V. Oscillations in Phanerozoic seawater chemistry: Evidence from fluid inclusions. *Science* **294**, 1086–1088 (2001).

12. Ridgwell, A. & Zeebe, R. E. The role of the global carbonate cycle in the regulation and evolution of the Earth system. *Earth and Planetary Science Letters* **234**, 299–315 (2005).

13. Zeebe, R. E. & Westbroek, P. A simple model for the CaCO3 saturation state of the ocean: The "Strangelove," the "Neritan," and the "Cretan" Ocean. *Geochemistry, Geophysics, Geosystems* **4**, (2003).

14. Copper, P. Ancient reef ecosystem expansion and collapse. *Coral Reefs* **13**, 3–11 (1994).

15. Dopieralska, J. Reconstructing seawater circulation on the Moroccan shelf of Gondwana during the Late Devonian: Evidence from Nd isotope composition of conodonts. *Geochemistry, Geophysics, Geosystems* **10**, (2009).

16. Jakubowicz, M. *et al.* At the southern limits of the Devonian reef zone: Palaeoecology of the Aferdou el Mrakib reef (Givetian, eastern Anti-Atlas, Morocco). *Geological Journal* **54**, 10–38 (2019).

17. Oczlon, M. S. Ocean currents and unconformities: The North Gondwana Middle Devonian. *Geology* **18**, 509–512 (1990).

18. Copper, P. Reef development at the Frasnian/Famennian mass extinction boundary. *Palaeogeography, Palaeoclimatology, Palaeoecology* **181**, 27–65 (2002).

19. McGhee, G. R., Sheehan, P. M., Bottjer, D. J. & Droser, M. L. Ecological ranking of Phanerozoic biodiversity crises: ecological and taxonomic severities are decoupled. *Palaeogeography, Palaeoclimatology, Palaeoecology* **211**, 289–297 (2004).

20. Raup, D. M. & Sepkoski, J. J. Mass Extinctions in the Marine Fossil Record. *Science* **215**, 1501–1503 (1982).

21. Sallan, L. & Galimberti, A. K. Body-size reduction in vertebrates following the end-Devonian mass extinction. *Science* **350**, 812–815 (2015).

22. Zapalski, M. K., Nowicki, J., Jakubowicz, M. & Berkowski, B. Tabulate corals across the Frasnian/Famennian boundary: architectural turnover and its possible relation to ancient photosymbiosis. *Palaeogeography, Palaeoclimatology, Palaeoecology* **487**, 416–429 (2017).

23. Percival, L. M. E. *et al.* Pulses of enhanced continental weathering associated with multiple Late Devonian climate perturbations: Evidence from osmium-isotope compositions. *Palaeogeography, Palaeoclimatology, Palaeoecology* **524**, 240–249 (2019).

24. Zapalski, M. K. Evidence of photosymbiosis in Palaeozoic tabulate corals. *Proc. R. Soc. B* **281**, 20132663 (2014).

25. Blackall, L. L., Wilson, B. & Oppen, M. J. H. van. Coral—the world's most diverse symbiotic ecosystem. *Molecular Ecology* **24**, 5330–5347 (2015).

26. Tambutté, S. *et al.* Coral biomineralization: From the gene to the environment. *Journal of Experimental Marine Biology and Ecology* **408**, 58–78 (2011).

27. Macko, S. A., Fogel, M. L., Hare, P. E. & Hoering, T. C. Isotopic fractionation of nitrogen and carbon in the synthesis of amino acids by microorganisms. *Chemical Geology: Isotope Geoscience section* **65**, 79–92 (1987).

28. Bada, J. L., Schoeninger, M. J. & Schimmelmann, A. Isotopic fractionation during peptide bond hydrolysis. *Geochimica et Cosmochimica Acta* **53**, 3337–3341 (1989).

29. Ferrier-Pagès, C. & Leal, M. C. Stable isotopes as tracers of trophic interactions in marine mutualistic symbioses. *Ecology and Evolution* **9**, 723–740 (2019).

30. Frankowiak, K. *et al.* Photosymbiosis and the expansion of shallow-water corals. *Sci. Adv.* **2**, e1601122 (2016).

31. Gannes, L. Z., O'Brien, D. M. & Rio, C. M. del. Stable Isotopes in Animal Ecology: Assumptions, Caveats, and a Call for More Laboratory Experiments. *Ecology* **78**, 1271–1276 (1997).

32. Muscatine, L. & D'Elia, C. F. The uptake, retention, and release of ammonium by reef corals 1. *Limnology and Oceanography* **23**, 725–734 (1978).

33. Wang, X. T. *et al.* Isotopic composition of carbonate-bound organic nitrogen in deep-sea scleractinian corals: A new window into past biogeochemical change. *Earth and Planetary Science Letters* **400**, 243–250 (2014).

34. Wang, X. T. *et al.* Influence of open ocean nitrogen supply on the skeletal δ15N of modern shallow-water scleractinian corals. *Earth and Planetary Science Letters* **441**, 125–132 (2016).

35. Wang, X. T. *et al.* Isotopic composition of skeleton-bound organic nitrogen in reef-building symbiotic corals: A new method and proxy evaluation at Bermuda. *Geochimica et Cosmochimica Acta* **148**, 179–190 (2015).

36. Muscatine, L. *et al.* Stable isotopes (13C and 15N) of organic matrix from coral skeleton. *Proceedings of the National Academy of Sciences* **102**, 1525–1530 (2005).

37. Auderset, A. *et al.* Enhanced ocean oxygenation during Cenozoic warm periods. *Nature* **609**, 77–82 (2022).

38. Kast, E. R. *et al.* Cenozoic megatooth sharks occupied extremely high trophic positions. *Science Advances* **8**, eabl6529 (2022).

39. Kast, E. R. *et al.* Nitrogen isotope evidence for expanded ocean suboxia in the early Cenozoic. *Science* **364**, 386–389 (2019).

40. Martínez-García, A. *et al.* Laboratory Assessment of the Impact of Chemical Oxidation, Mineral Dissolution, and Heating on the Nitrogen Isotopic Composition of Fossil-Bound Organic Matter. *Geochemistry, Geophysics, Geosystems* **23**, e2022GC010396 (2022).

41. Tornabene, C., Martindale, R. C., Wang, X. T. & Schaller, M. F. Detecting Photosymbiosis in Fossil Scleractinian Corals. *Scientific Reports* **7**, 9465 (2017).

42. Wang, X. T. *et al.* Oceanic nutrient rise and the late Miocene inception of Pacific oxygen-deficient zones. *Proceedings of the National Academy of Sciences* **119**, e2204986119 (2022).

43. Campoy, A. N. *et al.* The Origin and Correlated Evolution of Symbiosis and Coloniality in Scleractinian Corals. *Frontiers in Marine Science* **7**, (2020).

44. Swart, P. K. Carbon and oxygen isotope fractionation in scleractinian corals: a review. *Earth-Science Reviews* **19**, 51–80 (1983).

45. Barbeitos, M. S., Romano, S. L. & Lasker, H. R. Repeated loss of coloniality and symbiosis in scleractinian corals. *PNAS* **107**, 11877–11882 (2010).

46. Poty, E. Morphological limits to diversification of the rugose and tabulate corals. *Palaeoworld* **19**, 389–400 (2010).

47. LaJeunesse, T. *et al.* Closely related Symbiodinium spp. differ in relative dominance in coral reef host communities across environmental, latitudinal and biogeographic gradients. *Mar. Ecol. Prog. Ser.* **284**, 147–161 (2004).

48. Reuter, M., Brachert, T. C. & Kroeger, K. F. Diagenesis of growth bands in fossil scleractinian corals: identification and modes of preservation. *Facies* **51**, 146–159 (2005).

49. Jakubowicz, M. *et al.* Stable Isotope Signatures of Middle Palaeozoic Ahermatypic Rugose Corals – Deciphering Secondary Alteration, Vital Fractionation Effects, and Palaeoecological Implications. *PLOS ONE* **10**, e0136289 (2015).

50. Frankowiak, K., Mazur, M., Gothmann, A. M. & Stolarski, J. Diagenetic alteration of triassic coral from the aragonite konservat-lagerstätte in alakir çay, Turkey: Implications for geochemical measurements. *PALAIOS* **28**, 333–342 (2013).

51. Stanton Jr., R. J. Nutrient Models for the Development and Location of Ancient Reefs. *Geo.Alp* **3**, 191–206 (2006).

52. Algeo, T. J., Meyers, P. A., Robinson, R. S., Rowe, H. & Jiang, G. Q. Icehouse–greenhouse variations in marine denitrification. *Biogeosciences* **11**, 1273–1295 (2014).

53. Percival, L. M. E. *et al.* Combined Nitrogen-Isotope and Cyclostratigraphy Evidence for Temporal and Spatial Variability in Frasnian–Famennian Environmental Change. *Geochemistry, Geophysics, Geosystems* **23**, e2021GC010308 (2022).

54. Martinez-Garcia, A. *et al.* Iron Fertilization of the Subantarctic Ocean During the Last Ice Age. *Science* **343**, 1347–1350 (2014).

55. Ren, H. *et al.* Impact of glacial/interglacial sea level change on the ocean nitrogen cycle. *Proc Natl Acad Sci USA* **114**, E6759–E6766 (2017).

56. Ren, H. *et al.* Foraminiferal Isotope Evidence of Reduced Nitrogen Fixation in the Ice Age Atlantic Ocean. *Science* **323**, 244–248 (2009).

57. Robinson, R. S. *et al.* A review of nitrogen isotopic alteration in marine sediments. *Paleoceanography* **27**, (2012).

58. Straub, M. *et al.* Changes in North Atlantic nitrogen fixation controlled by ocean circulation. *Nature* **501**, 200–203 (2013).

59. Studer, A. S. *et al.* Ice Age-Holocene Similarity of Foraminifera-Bound Nitrogen Isotope Ratios in the Eastern Equatorial Pacific. *Paleoceanography and Paleoclimatology* **36**, e2020PA004063 (2021).

60. Ebneth, S., Diener, A., Buhl, D. & Veizer, J. Strontium isotope systematics of conodonts: Middle Devonian, Eifel Mountains, Germany. *Palaeogeography, Palaeoclimatology, Palaeoecology* **132**, 79–96 (1997).

61. Duprey, N. N. *et al.* Megacity development and the demise of coastal coral communities: Evidence from coral skeleton δ15N records in the Pearl River estuary. *Global Change Biology* **26**, 1338–1353 (2020).

62. Wang, X. T. *et al.* Isotopic composition of skeleton-bound organic nitrogen in reef-building symbiotic corals: A new method and proxy evaluation at Bermuda. *Geochimica et Cosmochimica Acta* **148**, 179–190 (2015).

63. Conti-Jerpe, I. E. *et al.* Trophic strategy and bleaching resistance in reef-building corals. *Sci. Adv.* **6**, eaaz5443 (2020).

64. Löw, M. *et al.* The initial phase of the Hönne Valley Reef at Binolen (northern Rhenish Massif, Middle Devonian). *Palaeobio Palaeoenv* (2022) doi:10.1007/s12549-022-00540-4.

65. Radice, V. Z., Hoegh-Guldberg, O., Fry, B., Fox, M. D. & Dove, S. G. Upwelling as the major source of nitrogen for shallow and deep reef-building corals across an oceanic atoll system. *Functional Ecology* **33**, 1120–1134 (2019).

66. Baker, D. M., Webster, K. L. & Kim, K. Caribbean octocorals record changing carbon and nitrogen sources from 1862 to 2005. *Global Change Biology* **16**, 2701–2710 (2010).

67. Erler, D. V. *et al.* Nitrogen isotopic composition of organic matter from a 168 year-old coral skeleton: Implications for coastal nutrient cycling in the Great Barrier Reef Lagoon. *Earth and Planetary Science Letters* **434**, 161–170 (2016).

68. Ren, H. *et al.* 21st-century rise in anthropogenic nitrogen deposition on a remote coral reef. *Science* **356**, 749–752 (2017).

69. Knapp, A. N., DiFiore, P. J., Deutsch, C., Sigman, D. M. & Lipschultz, F. Nitrate isotopic composition between Bermuda and Puerto Rico: Implications for N2 fixation in the Atlantic Ocean. *Global Biogeochemical Cycles* **22**, (2008).

70. Marconi, D. *et al.* Tropical Dominance of N2 Fixation in the North Atlantic Ocean. *Global Biogeochemical Cycles* **31**, 1608–1623 (2017).

71. Cline, J. D. & Kaplan, I. R. Isotopic fractionation of dissolved nitrate during denitrification in the eastern tropical north pacific ocean. *Marine Chemistry* **3**, 271–299 (1975).

72. Fripiat, F. *et al.* The Impact of Incomplete Nutrient Consumption in the Southern Ocean on Global Mean Ocean Nitrate δ15N. *Global Biogeochemical Cycles* **37**, e2022GB007442 (2023).

73. Fripiat, F. *et al.* Nitrogen isotopic constraints on nutrient transport to the upper ocean. *Nat. Geosci.* **14**, 855–861 (2021).

74. Knapp, A. N., Sigman, D. M. & Lipschultz, F. N isotopic composition of dissolved organic nitrogen and nitrate at the Bermuda Atlantic Time-series Study site. *Global Biogeochemical Cycles* **19**, (2005).

75. Casciotti, K. L. Inverse kinetic isotope fractionation during bacterial nitrite oxidation. *Geochimica et Cosmochimica Acta* **73**, 2061–2076 (2009).

76. Marshall, T. A. *et al.* The Agulhas Current Transports Signals of Local and Remote Indian Ocean Nitrogen Cycling. *Journal of Geophysical Research: Oceans* **128**, e2022JC019413 (2023).

77. Deutsch, C., Sarmiento, J. L., Sigman, D. M., Gruber, N. & Dunne, J. P. Spatial coupling of nitrogen inputs and losses in the ocean. *Nature* **445**, 163–167 (2007).

78. Hu, Y. & Fu, Q. Observed poleward expansion of the Hadley circulation since 1979. *Atmospheric Chemistry and Physics* **7**, 5229–5236 (2007).

79. Lucas, C., Timbal, B. & Nguyen, H. The expanding tropics: a critical assessment of the observational and modeling studies. *WIREs Climate Change* **5**, 89–112 (2014).

80. Brandes, J. A. & Devol, A. H. A global marine-fixed nitrogen isotopic budget: Implications for Holocene nitrogen cycling. *Global Biogeochemical Cycles* **16**, 67-1-67–14 (2002).

81. Becker, R., Dr. Aboussalam, Z., Stichling, S., May, A. & Eichholt, S. The Givetian-Frasnian Hönne Valley Reef Complex (northern Sauerland) - an outline of stratigraphy and facies development. *Münstersche Forschungen zur Geologie und Paläontologie* **108**, 126–140 (2016).

82. Schröder, S. & Salerno, C. Korallenfauna und Fazies givetischer Kalksteinabfolgen (Cürten-/Dreimühlen-Formation) der Dollendorfer Mulde (Devon, Rheinisches Schiefergebirge/Eifel). *Senckenbergiana Lethaea* **81**, 111–133 (2001).

83. Stadelmaier, M. *et al.* Ästige tabulate Korallen-Gemeinschaften aus dem Mitteldevon der Sötenicher Mulde (Eifel). Faunenzusammensetzung und fazielles Umfeld. (2005).

84. Birenheide, R. *Rugose Korallen des Devon.* vol. 2 (Leitfossilien, 1978).

85. Birenheide, R. *Chaetetida und tabulate Korallen des Devon*. vol. 3 (Leitfossilien, 1985).

86. Schröder, S. Stratigraphie und Systematik rugoser Korallen aus dem Givetium und Unter-Frasnium des Rheinischen Schiefergebirges (Sauerland/Bergisches Land). *Zitteliana* 39–116 (2005) doi:10.5282/ubm/epub.12134.

87. Ellison, S. The Composition of Conodonts. *Journal of Paleontology* **18**, 133–140 (1944).

88. Rejebian, V. A., Harris, A. G. & Huebner, J. S. Conodont color and textural alteration: an index to regional metamorphism, contact metamorphism, and hydrothermal alteration. *Geological Society of America Bulletin* vol. 99 9 (1987).

89. Epstein, A. G., Epstein, J. B. & Harris, L. D. Conodont Color Alteration- an Index to Organic Metamorphism. *Geological Survey Professional Paper* 995 (1977).

90. Nicoll, R. S. & Gorter, J. D. Conodont colour alteration, thermal maturation and the geothermal history of the Canning Basin, western Australia. *The APPEA Journal* **24**, 243–258 (1984).

91. Legall, F. D., Barnes, C. R. & Macqueen, R. W. Thermal maturation, burial history and hotspot development, Paleozoic strata of Southern Ontario-Quebec, from conodont and acritarch colour alteration studies. *Bulletin of Canadian Petroleum Geology* **29**, 492–539 (1981).

92. Harris, A. G. *et al. Conodont color alteration index (CAI) map and conodont-based age determinations for the Winchester 30' x 60' Quadrangle and adjacent area, Virginia, West Virginia, and Maryland. Conodont color alteration index (CAI) map and conodont-based age determinations for the Winchester 30' x 60' Quadrangle and adjacent area, Virginia, West Virginia, and Maryland* vol. 2239 http://pubs.er.usgs.gov/publication/mf2239 (1994).

93. Helsen, S. & Königshof, P. Conodont thermal alteration patterns in Palaeozoic rocks from Belgium, northern France and western Germany. *Geological Magazine* **131**, 369–386 (1994).

94. Garcia-Lopez, S., Brime, C., Bastida, F. & Sarmiento, G. N. Simultaneous use of thermal indicators to analyse the transition from diagenesis to metamorphism: an example from the Variscan Belt of northwest Spain. *Geological Magazine* **134**, 323–334 (1997).

95. Sarmiento, G. N., García-lópez, S. & Bastida, F. Conodont colour alteration indices (CAI) of Upper Ordovician limestones from the Iberian Peninsula. *Geologie en Mijnbouw* **77**, 77–91 (1998).

96. Lazreq, N. & Ali, B. Discovery of Upper Devonian conodonts and event stratigraphy from the Eastern Jebilet, Morocco. *Journal of African Earth Sciences* **196**, 104699 (2022).

97. Königshof, P. Der Farbänderungsindex von Conodonten (CAI) in paläozoischen - Gesteinen (Mitteldevon bis Unterkarbon) des Rheinischen - Schiefergebirges. https://www.schweizerbart.de/publications/detail/isbn/9783510611225/CFS_Courier_Forschungsinstitut_Senckenbe?l=DE (1992).

98. Königshof, P. Deformationsstrukturen und texturelle Veränderung paläozoischer Conodonten: Beispiele aus Deutschland und Frankreich. *Senckenbergiana Lethaea* **83**, 149–156 (2003).

99. Raven, J. G. M. & Pluijm, B. A. V. D. Metamorphic fluids and transtension in the Cantabrian Mountains of northern Spain: an application of the conodont colour alteration index. *Geological Magazine* **123**, 673–681 (1986).

100. Sigman, D. M. *et al.* A Bacterial Method for the Nitrogen Isotopic Analysis of Nitrate in Seawater and Freshwater. *Anal. Chem.* **73**, 4145–4153 (2001).

101. Wang, X. T. *et al.* Isotopic composition of skeleton-bound organic nitrogen in reef-building symbiotic corals: A new method and proxy evaluation at Bermuda. *Geochimica et Cosmochimica Acta* **148**, 179–190 (2015).

102. Moretti, S. *et al. Analytical improvements and assessment of long-term performance of the oxidation-denitrifier method*. https://essopenarchive.org/users/558394/articles/648017-analytical-improvements-and-assessment-of-long-term-performance-of-the-oxidation-denitrifier-method?commit=bdb84bff3584e165cc9cd8611e61a6dd73b47d4f (2023) doi:10.22541/au.168616993.39320235/v1.

103. Braman, R. S. & Hendrix, S. A. Nanogram nitrite and nitrate determination in environmental and biological materials by vanadium(III) reduction with chemiluminescence detection. *Anal. Chem.* **61**, 2715–2718 (1989).

104. Weigand, M. A., Foriel, J., Barnett, B., Oleynik, S. & Sigman, D. M. Updates to instrumentation and protocols for isotopic analysis of nitrate by the denitrifier method. *Rapid Communications in Mass Spectrometry* **30**, 1365–1383 (2016).

105. McGregor, H. V. & Gagan, M. K. Diagenesis and geochemistry of porites corals from Papua New Guinea: Implications for paleoclimate reconstruction. *Geochimica et Cosmochimica Acta* **67**, 2147–2156 (2003).

106. Müller, A., Gagan, M. K. & McCulloch, M. T. Early marine diagenesis in corals and geochemical consequences for paleoceanographic reconstructions. *Geophysical Research Letters* **28**, 4471–4474 (2001).

107. Sayani, H. R. *et al.* Effects of diagenesis on paleoclimate reconstructions from modern and young fossil corals. *Geochimica et Cosmochimica Acta* **75**, 6361–6373 (2011).

108. Swart, P. K. The geochemistry of carbonate diagenesis: The past, present and future. *Sedimentology* **62**, 1233–1304 (2015).

109. Hendy, E. J., Gagan, M. K., Lough, J. M., McCulloch, M. & deMenocal, P. B. Impact of skeletal dissolution and secondary aragonite on trace element and isotopic climate proxies in Porites corals. *Paleoceanography* **22**, (2007).

110. McGregor, H. V. & Gagan, M. K. Diagenesis and geochemistry of porites corals from Papua New Guinea: Implications for paleoclimate reconstruction. *Geochimica et Cosmochimica Acta* **67**, 2147–2156 (2003).

111. Hudson, J. D. Stable isotopes and limestone lithification. *Journal of the Geological Society* **133**, 637–660 (1977).

112. Stanley, G. D. & Swart, P. K. Evolution of the Coral-Zooxanthenllae Symbiosis During the Triassic: A Geochemical Approach. *Paleobiology* **21**, 179–199 (1995).

113. Munro, L. E., Longstaffe, F. J. & White, C. D. Effects of heating on the carbon and oxygen-isotope compositions of structural carbonate in bioapatite from modern deer bone. *Palaeogeography, Palaeoclimatology, Palaeoecology* **266**, 142–150 (2008).

114. Schrag, D. P., DePaolo, D. J. & Richter, F. M. Reconstructing past sea surface temperatures: Correcting for diagenesis of bulk marine carbonate. *Geochimica et Cosmochimica Acta* **59**, 2265–2278 (1995).

115. Derrick, B. & White, P. Why Welch's test is Type I error robust. *TQMP* **12**, 30–38 (2016).

116. Ruxton, G. D. The unequal variance t-test is an underused alternative to Student's t-test and the Mann–Whitney U test. *Behavioral Ecology* **17**, 688–690 (2006).
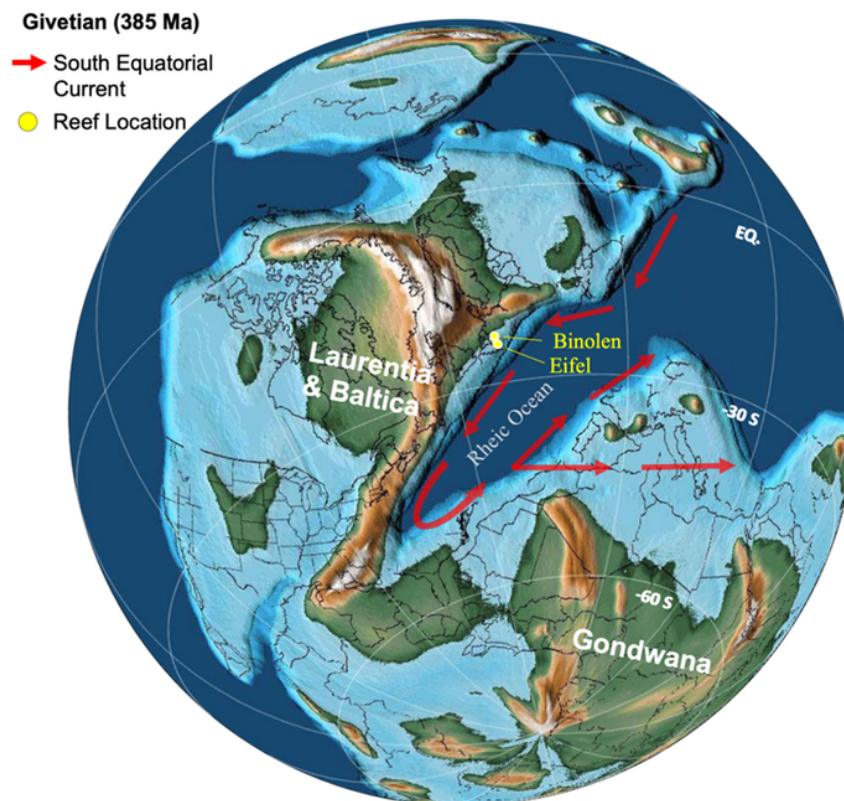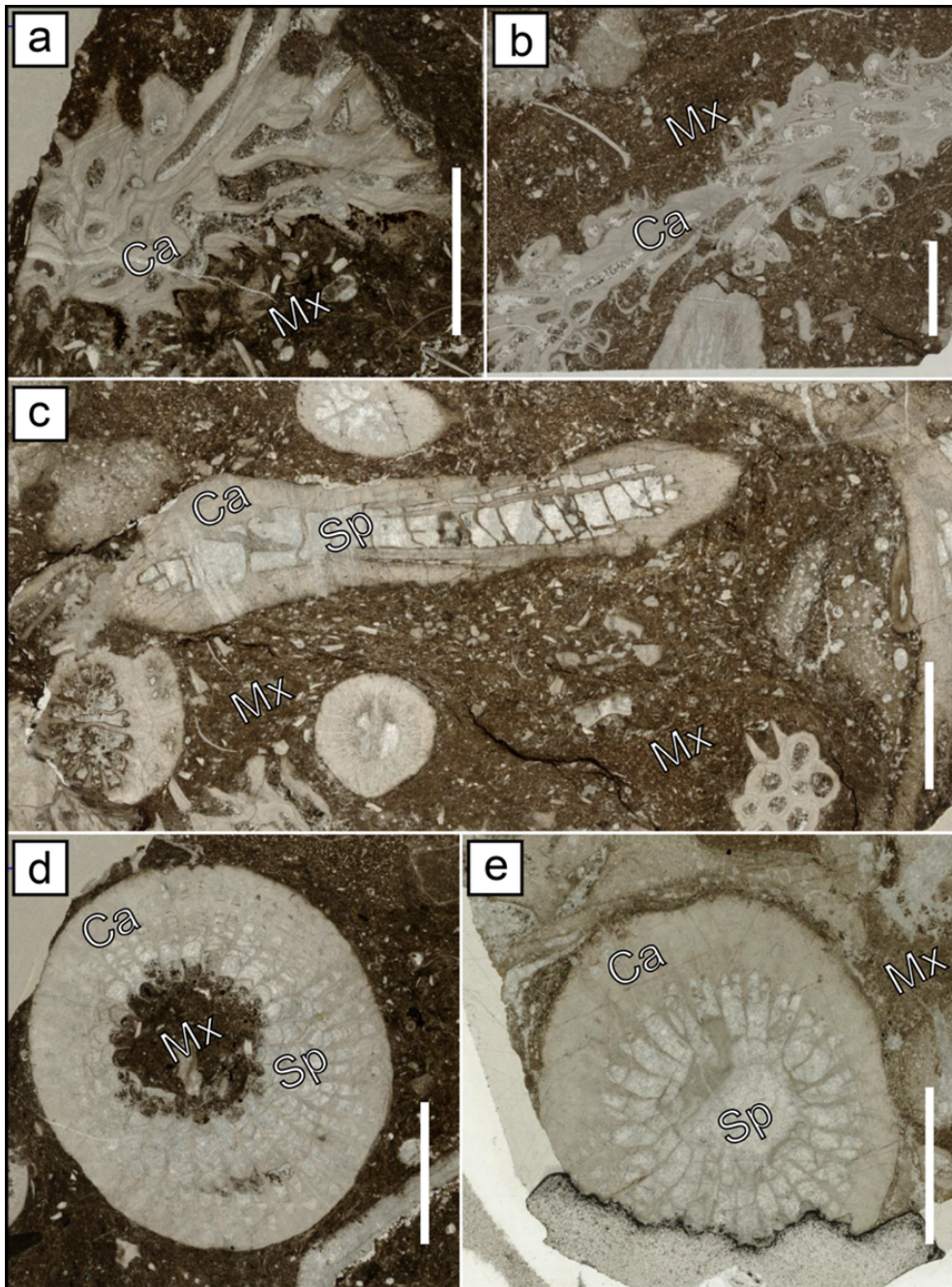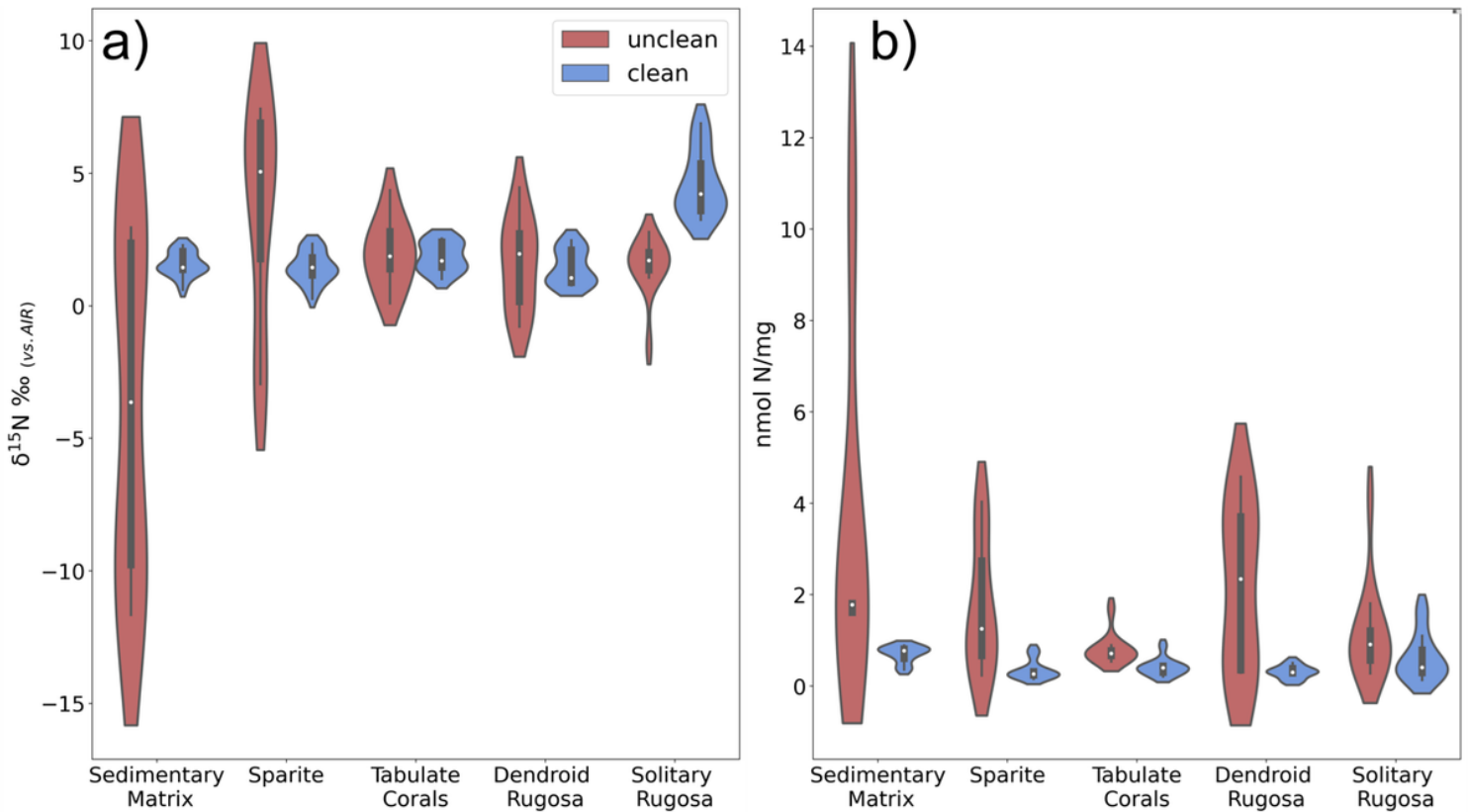
Figures

Figure 1

Paleogeographic reconstruction of the continental configuration during the Givetian stage (~387–382 Ma) of the Devonian Period (~419–359 Ma). The paleo map and paleo positions were generated using GPlates based on the PALEOMAP project (Scotese, 2016). The south equatorial current is based on reconstructions and iterations by Dopieralska (2009), Jakubowicz et al. (2019) and Oczlon (1990). Sampling locations are indicated in yellow.
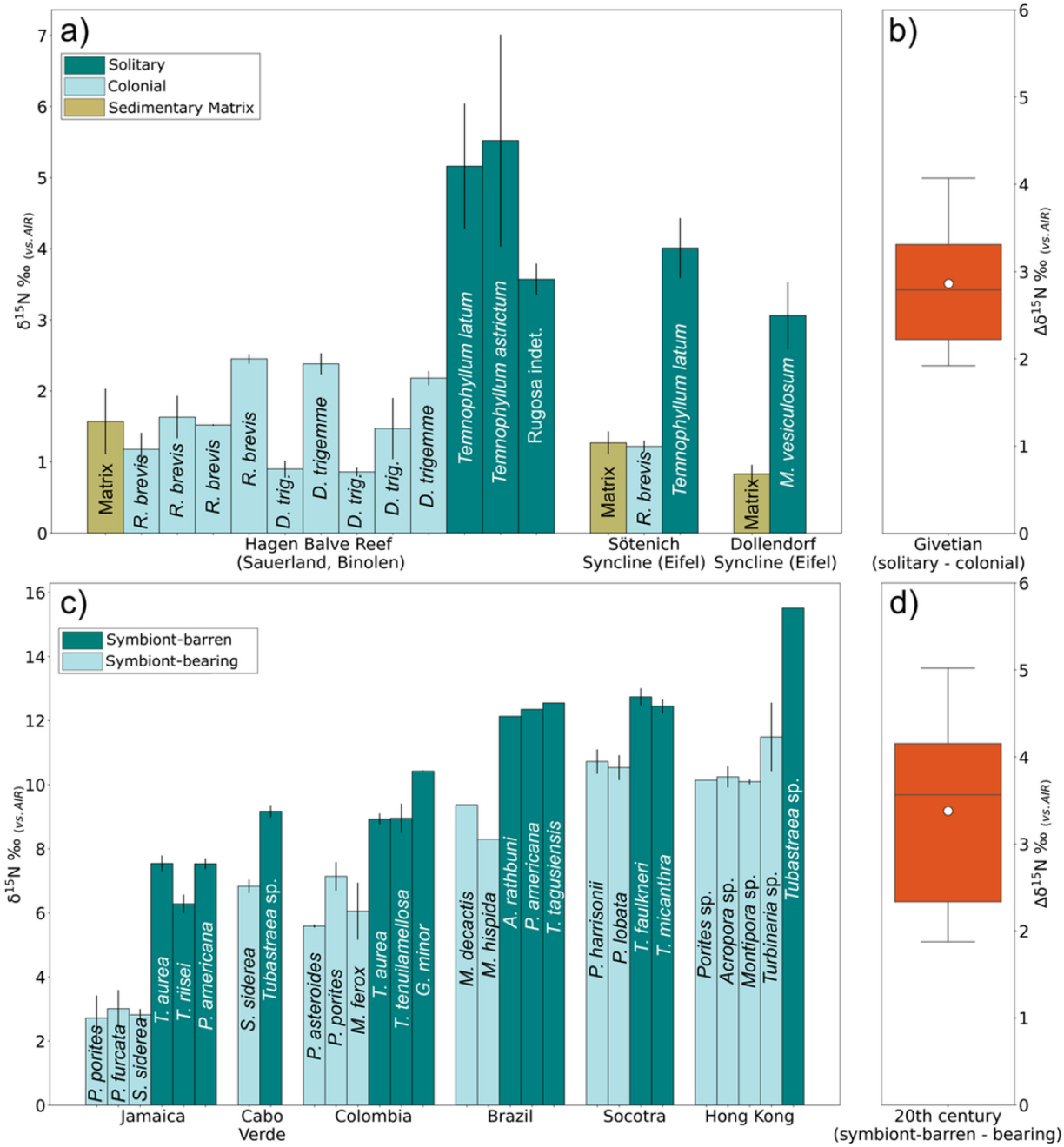

Figure 2

Microphotographs of thin sections (under transmitted light) of corals from the initial Hagen Balve Reef (lower/middle Givetian) from the Binolen locality of the Sauerland area. **a)** Anastomosing branch of tabulate (auloporid) coral *Roemerolites brevis rhiphaeus* (GMM B2C.59-2). **b)** Branch of *R. brevis rhiphaeus* with calices partly filled with sediment and/or sparite (GMM B2C.59-3). **c)** Longitudinal and cross-sections of loosely-colonial (dendroid) rugose coral *Dendrostella trigemme* and fragments of *R. brevis rhiphaeus* (GMM B2C.59-4). One cross-section of *D. trigemme* (lower left) shows species-specific dendroid astogeny. **d)** Cross-section through calyx of the solitary rugose coral *Temnophyllum astrictum* with species-specific incompletely developed peripheral wall (same thin section as 2a). Calyx center is filled with sediment,

whereas spaces between septa and dissepiments are filled with sparite. **e)** Cross section through the solitary rugose coral *Temnophyllum latum* with calyx filled with sparite (GMM B2C.59-9). In contrast to *T. astrictum*, the thick peripheral wall of *T. latum* is nearly completely developed. All thin sections belong to a microfacies type described by Löw et al. (2022) as coral-stromatoporoid baffle-floatstones (their MF8 including subtypes), representing deposits of an initial reef platform of the Hagen-Balve Reef. Ca: calcium carbonate, Sp: sparite, Mx: sedimentary matrix. Scale bars: 5 mm.

Figure 3

a) Coral-bound nitrogen isotope values of three distinct coral groups and their surrounding material from the Hagen Balve Reef (in ‰ vs. air). Clean and unclean material yield a significant difference for the sediment, sparite and solitary rugose corals but not for dendroid rugose corals or tabulate corals. Cleaned samples converge to mean values between 0.78‰ and 2.48‰ for colonial corals (tabulate and dendroid rugose corals) and are significantly different to the solitary rugose coral samples ($P < 0.01$). Mean values are indicated by the white dots. **b)** Corresponding weight-normalized nitrogen content (in nmol N per mg of carbonate powder) is given. Overall, nitrogen content is very low but always higher in unclean samples.

Figure 4

a) Cleaned coral-bound nitrogen isotope values (in ‰ vs. air) of sedimentary matrix, tabulate (*Romerolites brevis rhiphaeus/brevis*), dendroid rugose corals (*Dendrostella trigemme*), and solitary rugose corals (*Temnophyllum latum, Temnophyllum astricum and Mesophylum vesiculosum*) from the Hagen Balve Reef in Binolen as well as the Sötenich Syncline and Dollendorf Syncline of the Eifel region. Cleaned sedimentary matrix, and colonial coral species converge to mean $\delta^{15}N$ = 1.40‰, 1.27‰ and 0.83‰ for Binolen, the Sötenich and Dollendorf Syncline, respectively. Solitary species show average $\delta^{15}N$ values of 3.38‰ and 4.62‰ for the Eifel and Hagen Balve Reef, respectively **b)** Average difference (expressed as $\Delta\delta^{15}N = \delta^{15}N_{non-sym./solitary} - \delta^{15}N_{sym/colonial/matrix}$) between solitary and colonial species or matrix material from the three reef formations. **c)** $\delta^{15}N$ of symbiont-bearing species and symbiont-barren species for various locations taken from the same reef depth and time. Individual species are listed where several measurements of the same species are taken together and the respective intraspecies variation is shown by vertical bars. **d)** Average difference between symbiont-barren and symbiont-bearing species from all locations.

Supplementary Files

This is a list of supplementary files associated with this preprint. Click to download.

- ExtendedDataFiguresandSuppTables.docx